New Organic–Inorganic Hybrid Membranes Based on Sulfonated Polyimide/Aminopropyltriethoxysilane Doping with Sulfonated Mesoporous Silica for Direct Methanol Fuel Cells

Lei Geng, Yao He, Dan Liu, Changli Lü

College of Chemistry, Northeast Normal University, Changchun 130024, People's Republic of China

Received 13 February 2011; accepted 24 May 2011
DOI 10.1002/app.34978
Published online 2 September 2011 in Wiley Online Library (wileyonlinelibrary.com).

ABSTRACT: A series of novel composite methanol-blocking polymer electrolyte membranes based on sulfonated polyimide (SPI) and aminopropyltriethoxysilane (APTES) doping with sulfonated mesoporous silica (S-mSiO_2) were prepared by the casting procedure. The microstructure and properties of the resulting hybrid membranes were extensively characterized. The crosslinking networks of amino silica phase together with sulfonated mesoporous silica improved the thermal stability of the hybrid membranes to a certain extent in the second decomposition temperature (250–400°C). The composite membranes doping with sulfonated mesoporous silica (SPI/APTES/S-mSiO_2) displayed superior comprehensive performance to the SPI and SPI/APTES membranes, in which the homogeneously embedded S-mSiO_2 provided new pathways for proton conduction, rendered more tortuous pathways as well as greater resistance for methanol crossover. The hybrid membrane with 3 wt % S-mSiO_2 into SPI/APTES-4 (SPI/A-4) exhibited the methanol permeability of 4.68×10^{-6} cm^2 s^{-1}at 25°C and proton conductivity of 0.184 S cm^{-1} at 80°C and 100%RH, while SPI/A-4 membrane had the methanol permeability of 5.16×10^{-6} cm^2 s^{-1} at 25°C and proton conductivity of 0.172 S cm^{-1} at 80°C and 100%RH and Nafion 117 exhibited the values of 8.80×10^{-6} cm^2 s^{-1} and 0.176 S cm^{-1} in the same test conditions, respectively. The hybrid membranes were stable up to about 80°C and demonstrated a higher ratio of proton conductivity to methanol permeability than that of Nafion117. © 2011 Wiley Periodicals, Inc. J Appl Polym Sci 123: 3164–3172, 2012

Key words: organic–inorganic crosslinked electrolyte membrane; sulfonated mesoporous silica; sulfonated polyimide; direct methanol fuel cells

INTRODUCTION

Proton exchange membrane fuel cells (PEMFCs) have attracted much attention as a clean energy source because of their high energy density and efficiency for various applications such as electric vehicles, portable electronics, and residential power generation.[1–6] The polymer electrolyte membrane (PEM), which acts as an electrolyte to transport protons from the anode to the cathode, is one of the key components of polymer electrolyte membrane fuel cells.[7] A series of perfluorosulfonate ionomers, such as Nafion, are the most widely used proton exchange membranes in direct methanol fuel cells, because of their high proton conductivity, excellent chemical and physical properties. However, the high cost, low operation temperature and high fuel crossover as well as other problems have limited their practical application in fuel cells.[8–11] Therefore, it is strongly desired to develop new proton exchange membrane materials with lower cost and high performance.

Currently, many efforts to design alternative Nafion have been made and the intense research focused on various sulfonated polymers, such as sulfonated poly(aryl ether ketone)s, sulfonated polysulfones, sulfonated poly-benzimidazoles, sulfonated polyimides, and so on.[12–15] Generally, the membranes based on these polymers only reach high proton conduction at high ion-exchange capacity (IEC). However, when IEC increases, the membranes become more swollen, show excessive reactant crossover, and lose the mechanical stability.

To improve the mechanical stability of the pure polymer membrane with high IEC, some methods were used, such as fabricating composite

Correspondence to: C. Lü (lucl055@nenu.edu.cn).
Contract grant sponsor: National Natural Science Foundation of China; contract grant numbers: 20704004, 21074019.
Contract grant sponsor: Natural Science Foundation of Jilin Province; contract grant number: 20101539.
Contract grant sponsor: Jilin Province Science and Technology Development Project; contract grant number: 20090155.
Contract grant sponsor: China Postdoctoral Science Foundation Funded Project; contract grant number: 200904501024.

membranes[16–20] and optimizing the polymer structure.[21–25] Organic–inorganic hybrid is one of the most promising materials for the proton exchange membranes because of its capacity to produce materials having a wide range of physical, chemical, thermal, and mechanical properties based on the beneficial properties of organic and inorganic phase.[26] The cross-linking strategy for the proton exchange membranes is promising because of its easy preparation. The interactions between the acidic and basic components, such as ionic-crosslinking (electrostatic forces) and hydrogen-bond bridges can be used to control dimensional swelling without decrease in flexibility. The resulting membranes are expected to have low water uptake, reduced reactant crossover, good thermal stability, high mechanical strength, and flexibility. Many studies have been done to use the cross-linking method in the area of PEMs. Kim et al. reported the preparation of sulfonated PESs with crosslinked structure by thermal irradiation of the allyl-terminated PESs using a bisazide as a crosslinker.[27] Xu et al. recently reported the acid–base hybrid polymer electrolyte membranes based on the reaction of SPEEK or sulfonated poly(2,6-dimethyl-1,4-phenylene oxide) (SPPO) with APTES, and the acid–base interaction was proved to be effective for improving the thermal stability, homogeneity, and dimensional stability of the membranes.[9,28] Shul et.al prepared the semi-IPN (semi-interpenetrating polymer network) membrane by *in situ* polymerization and crosslinking of sodium salt of sulfonated styrene in the pores of Nafion 117.[29] However, in most of these cases, proton conductivity decreased significantly due to the diminishing free protons of conductive materials or the addition of nonconductive materials.

The mesoporous materials with high specific surface area and large open channels are paid attention due to their high chemical and thermal stability in recent years. Among mesoporous materials, mesoporous silica-based materials are of particular interest.[30–33] Besides, the pores of mesoporous silica can be modified by using amine, thiol, and sulfonic acid groups. Thus, mesoporous silica is an usual inorganic material that can be introduced into the polymers to improve the properties of the proton exchange membranes. Tominaga et al. prepared hexagonally ordered mesoporous silica as inorganic fillers, and they added it to Nafion to prepare composite membranes. The composite membranes had 1.5 times higher proton conductivities than pure Nafion at 80°C.[34] Lee et al. synthesized mesoporous silica sphere grafted with organic sulfonic acid, then proton-conducting organic–inorganic composite membranes were cast together with Nafion using these functionalized mesoporous silica as inorganic fillers. The composite membranes showed increased water uptake and higher ionic conductivity relative to recast Nafion membrane under low relative humidity condition.[35] Okamoto et al. prepared the sulfonated polyimide hybrid membranes by using sulfonated Si-MCM-41 as a hydrophilic and proton-conductive inorganic component. The SMCM/sulfonated polyimide hybrid membrane with 20 wt % loading of SMCM showed the high mechanical tensile strength and the slightly higher water vapor sorption than the host SPI membrane.[36]

Here, we used the sulfonated polyimides (SPIs) as the polyelectrolyte matrix to fabricate the organic–inorganic hybrid membranes. The aim of the present work is to improve the thermal stability, mechanical strength, swelling ability when testing proton conductivity at 80°C, suppress the methanol crossover while maintaining higher proton conductivity with a reasonable water uptake of the SPI-based membranes. The sulfonic acid group of sulfonated polyimides itself was used as a catalyst for sol–gel process of aminopropyltriethoxysilane (APTES) to form the crosslinked silica network. Meanwhile, there is the strong interaction between amine groups in APTES and sulfonic acid group in SPI. Then, a certain amount of sulfonated mesoporous silica nanoparticles was incorporated into the acid–base hybrid system by blending method. The existence of crosslinked silica network could increase the compatibility of sulfonated mesoporous silica with SPI by the interaction of hydroxyl groups on the surface of silica. The existence of crosslinked silica network and the sulfonated mesoporous silica improved the thermal properties to some extent, water-uptake, proton conductivity and methanol permeability of the resulting hybrid membranes as compared with that of pure SPI.

EXPERIMENTAL

Materials

1,4,5,8-naphthalenetetracarboxylic dianhydride (NTDA), 4,4′-diaminodiphenyl ether (ODA) were purchased from Tokyo Kasel, and purified by vacuo sublimation prior to use. 4,4′-diaminodiphenyl ether-2,2′-disulfonic Acid (ODADS) was synthesized using ODA as raw material by the method mentioned in literature.[37] Benzoic acid, concentrated hydrochloric acid, concentrated sulfuric acid (98%), acetone, ethanol, sodium hydroxide, hexadecyltrimethyl ammonium bromide (CTAB), 3-mercaptopropyltrimethoxysilane (MPTMS), hydrogen peroxide (33%), and fuming sulfuric acid were used as received. Aminopropyltriethoxysilane (APTES), dimethyl sulfoxide (DMSO), *m*-cresol and tetraethyl orthosilicate (TEOS) were distilled prior to use. Triethylamine(Et_3N) was

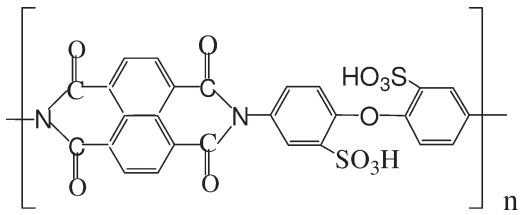

Scheme 1 Struture of sulfonated polyimide.

distilled and dried with 4 Å molecular sieves prior to use.

Synthesis of sulfonated polyimide

The chemical structure of sulfonated polyimide (SPI) is given in Scheme 1. 10.8 g (30 mmol) of ODADS, 100 mL of *m*-cresol, and 7.2 g (72 mmol) of triethylamine were mixed under nitrogen flow with stirring. After ODADS was completely dissolved, 8.04g (30 mmol) of NTDA and 5.2 g (42.6 mmol) of benzoic acid were added. The mixture was stirred at room temperature for a few minutes, and then heated at 80°C for 4 h and 180°C for 20 h. After cooling to 100°C, an additional 100 mL of *m*-cresol was added to dilute the viscous solution, which was then poured into acetone. The fiber-like precipitate was filtered off, washed with acetone, and dried in vacuo. IR (KBr, cm-1): 3394, 1710, 1670, 1584, 1468, 1348, 1250, 1192, 1080, 1024, 710; ^{1}H-NMR (DMSO-d6, Et_3N was added for dissolution in DMSO, ppm) : 8.73, 7.92, 7.45, 7.19, 7.00, 6.76, 6.55, 5.04.

Synthesis of sulfonated mesoporous silica nanoparticles (S-mSiO_2)

Totally, 10.6 mL 2*M* NaOH and 3.06 g CTAB were dissolved in 1440 mL water, the resulting solution was heated to 80°C, then the mixture of 15 mL TEOS, and 1.28 mL MPTMS was added to the solution under stirring and the reaction was kept at this temperature for 2 h. After the reaction, white precipitate was obtained by centrifugation. The precipitate was washed with deionized water for one time. Template extraction was performed with 60 mL conc. HCl in 480 mL ethanol. Usually, 1 g of sample was treated two to three times with 100 mL of the extraction solution by sonication for 30 min. Subsequent washing was performed as described above. After the extraction of template, the precipitate was added into concentrated hydrogen peroxide (33%) for 24 h in order to oxidate the mercapto groups of MPTMS segments to sulfonic groups. The final obtained samples were separated by centrifugation, washed with deionized water for three times and dried at 60°C under vacuum.

Preparation of SPI/ APTES and SPI/ APTES/S-mSiO_2 hybrid membranes

Totally, 0.5 g of SPI was added into 4.0 mL DMSO, and the mixture was heated to 150°C for several hours with stirring till the SPI dissolved. Then the solution was cooled to 30°C. The APTES and deionized water with a molar ratio of 1 : 4 were mixed together in DMSO. The above two solutions were blended and stirred for 2 h to prepare a uniform solution. By adjusting the adding amount of APTES, different SPI/APTES hybrid systems with 4, 7, and 15 wt % of APTES were obtained. Meanwhile, for preparing SPI/APTES/S-mSiO_2, 0.015 g S-mSiO_2 was added into DMSO and the mixture was sonicated for 30 min. Then the S-mSiO_2 in DMSO was added into the SPI/APTES solution, and the mixture was stirred for 1 h, and sonicated for 30 min. The membranes were formed by casting the above solution onto glass dishes, and dried at 80°C for 8 h, then heated at 150°C for 2 h, and 180°C for 6 h. When the membranes were cooled to room temperature, they were boiled in deionized water to be peeled off, and then dried in vacuum for 24 h. Through this method, a series of nanocomposite membranes were obtained. These membranes are defined as SPI/A-X/S-Y, where X and Y represent the weight percent of APTES and S-mSiO_2 in hybrid membranes, respectively.

Characterization and property measurements

Instrumental characterizations

Fourier transform infrared (FTIR) spectra were recorded using a Nicolet AVATAR360 spectrometer. Thermogravimetric analysis (TGA) was conducted utilizing a Perkin-Elmer TGA-2 thermogravimetric analyzer by heating the samples from ambient temperature to 800°C with a heating rate of 10°C/min in nitrogen. The morphologies of fractured surfaces of the hybrid membranes by brittle breakage using liquid nitrogen were studied using SEM (XL-30 ESEM FEG, FEI Company). The TEM characterization was carried using a JEM-2100F microscope. Nitrogen (N_2) adsorption/desorption isotherms were measured by using a Nova l000 analyzer with nitrogen. Surface areas were calculated by the Brunauer-Emmett-Teller (BET) method and pore sizes by the Barrett-Joyner-Halenda (BJH) methods. The tensile measurements of the dried membranes were carried out on an Instron model 1122 at a testing rate of 1 mm/min at room temperature and 30% relative humidity according to the standard GB/T 1040-1992. Each measurement was repeated five times to guarantee good reproducibility of results. Gas chromatography (GC) was performed on a SP-3400 AGILENT 6890.

Water uptake

Hybrid membrane samples were dried in a vacuum oven at 100°C for 6 h and weighted. Then the samples were immersed in distilled water for 24 h. The water uptake was calculated using the following equation:

$$\text{Water uptake WU} = \frac{W_{\text{wet}} - W_{\text{dry}}}{W_{\text{dry}}} \times 100\%,$$

where W_{wet} is the weight of wet membranes and W_{dry} is the weight of dried membranes.

Ion-exchange capacity

Ion-exchange capacity (mmol of sulfonic acid per gram of sample) of hybrid membranes was determined by the back-titration method. The membranes in acid form were converted to the sodium form by immersing the membranes in 1*M* NaCl solution for 24 h to exchange the H^+ ions for Na^+ ions. The exchanged H^+ ions within the solution were titrated with 0.005*M* NaOH solution with phenolphthalein as an indicator. The ion exchange capacities of membranes were calculated from the titration data by the following equation:

$$\text{IEC} = \frac{V_{\text{NaOH}} \times C_{\text{NaOH}}}{W_{\text{dry}}}$$

where W_{dry} is the dry weight of the sample in the H^+ form, V_{NaOH} is the titrated volume of the NaOH solution, and C_{NaOH} is the concentration of the NaOH solution.

Proton conductivity

Proton conductivity of full hydration membranes was measured in the lateral direction by AC impedance method using an electrochemical work station. The conductivity of the hybrid membranes was measured using a modified four-probe AC impedance method from 1 Hz to 100 kHz by sandwiching the membranes between two pairs of gold-plate electrodes. Before the test, the as-cast films were soaked in methanol at 60°C for 1 h to remove the residual solvent (DMSO), and then the proton exchange treatment was performed by immersing the membranes in 1.0*N* hydrochloric acid at room temperature for above 6 h. The membranes in proton form were then immersed in deionized water for 2 h. The conductivity of the membranes was calculated from the following equation:

$$\sigma = \frac{L}{\text{RA}},$$

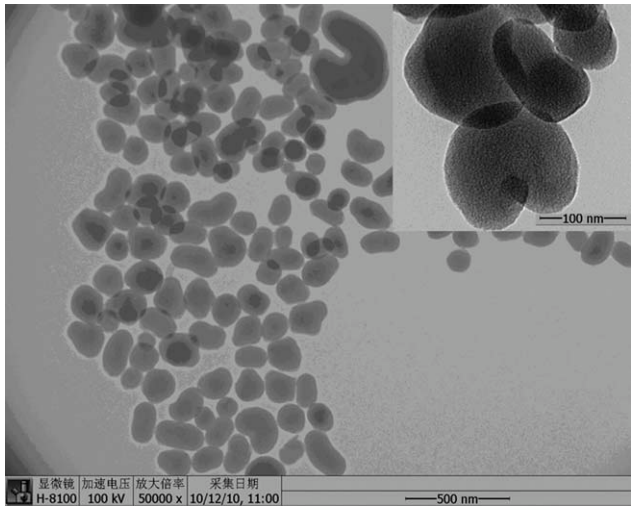

Figure 1 TEM images of S-mSiO_2. Inset is the expanded image of S-mSiO_2.

where σ is proton conductivity in S/cm, *L* is the distance between the two electrodes, *R* is resistance of the membrane, and *A* is the cross-sectional area of membrane.

Methanol permeability

Methanol permeability was measured using a liquid permeation cell, which was composed of two compartments of the same volume (50 mL). At the beginning, one compartment was filled with methanol, and the other one was filled with deionized water. The membrane sample was sandwiched between the two cells. When tested, both compartments were kept stirring during experiment to ensure the uniformity of the cell concentration. The stirring was kept for 24 h and then some amount of solution was got from the compartment which was filled with water at first. The methanol content of the solution was tested by gas chromatography (GC). Methanol permeability for 24 h was calculated using the following equation:

$$P = \frac{\text{QL}}{A},$$

where *Q* is the methanol volume that permeated through the membrane per second, *L* is the membrane thickness, and *A* is the surface area of the membrane.

RESULTS AND DISCUSSION

Synthesis and characterization of S-mSiO_2

Figure 1 shows the TEM micrographs of S-mSiO_2. The inset is the regular array of ordered mesopores expanded from a section of the silica shell, in which

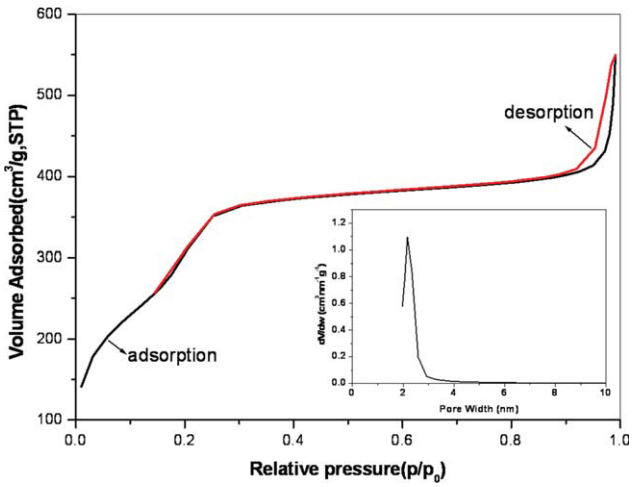

Figure 2 Nitrogen adsorption-desorption isotherms of S-$mSiO_2$. The inset is the corresponding BJH pore distribution. [Color figure can be viewed in the online issue, which is available at wileyonlinelibrary.com.]

the ordered mesopores of about 2.3 nm are clearly visible. On the whole, the S-$mSiO_2$ nanoparticles with a diameter of about 50–300 nm are dispersing homogeneously without any obvious aggregation.

Liquid nitrogen isotherm measurements are used to characterize the pore volume, pore size, and surface area of the S-$mSiO_2$ nanoparticles. The isotherm shown in Figure 2 is the type-IV isotherms according to the IUPAC classification. A well-defined step at intermediate relative pressure ($0.15 < P/P_0 < 0.25$) is related with the filling of the mesopores due to capillary condensation of N_2 inside the mesopores. The hysteresis loop appears at about 0.9 is probably due to the gaps among the inorganic particles. The surface area is determined using the Brunauer-Emmet-Teller (BET) equation to be 1019 m^2/g. The inset of Figure 2 is a pore width distribution graph indicating an average pore radius of 2.35 nm, which shows the uniformity of the mesoporous structure.

FTIR analysis

The FT-IR spectra of SPI and different nanocomposite membranes are shown in Figure 3. It can be seen that for SPI, the absorption peaks at 1714 and 1675 cm^{-1} belong to the stretching vibrations of carbonyl groups of imido rings. The absorption peak at 1348 cm^{-1} corresponds to the amino groups of aromatic rings, and this peak moves from 1250–1340 cm^{-1} to 1348 cm^{-1} due to the effect of electron-withdrawing sulfonic acid groups. The characteristic absorptions of sulfonic acid groups are observed at 3430, 1253, and 1084 cm^{-1}, corresponding to the O—H vibration of $\sim SO_3H$, the asymmetric O=S=O stretching and the superposition of symmetric O=S=O stretching, respectively. For the hybrid membrane SPI/A-15/S-3, the new bands appear at 1080 and 1643 cm^{-1}, which can be attributed to the Si—O—Si asymmetric and bending vibration of N—H of APTES, respectively. The characteristic peak of Si—O—Si confirms the presence of an extended siloxane network from the sol–gel condensation reaction of APTES and S-$mSiO_2$ in the hybrid membrane.

Microstructure

The SEM measurements were used to characterize the micro-structure of the SPI/APTES and SPI/APTES/S-$mSiO_2$ hybrid membranes. The SEM images of the hybrid membranes on cross-section are shown in Figure 4. From the SEM images, we can see when the amount of APTES is low (4 wt %), the polymer matrix is homogenous with no noticeable microphase separation with silica [Fig. 4(a)]. When the amount of APTES increases to 15 wt %, the aggregation of silica becomes evident [Fig. 4(c)]. The above phenomenon also is observed in the samples of SPI/A-4/S-3 and SPI/A-15/S-3, respectively. The Si mapping images of energy-dispersive spectrometer (EDS) of SPI/A-4/S-3 and SPI/A-15/S-3 are also shown in Figure 4. We can see that the Si element is dispersed uniformly in the whole organic matrix, no aggregation or gather can be observed in SPI/A-4/S-3[Fig. 4(e)], while in the sample SPI/A-15/S-3, Si element has some aggregation in the organic matrix, which is in accordance with the SEM images.

Thermogravimetric analysis

The thermal stabilities of SPI and their hybrid membranes were investigated and their TGA curves are

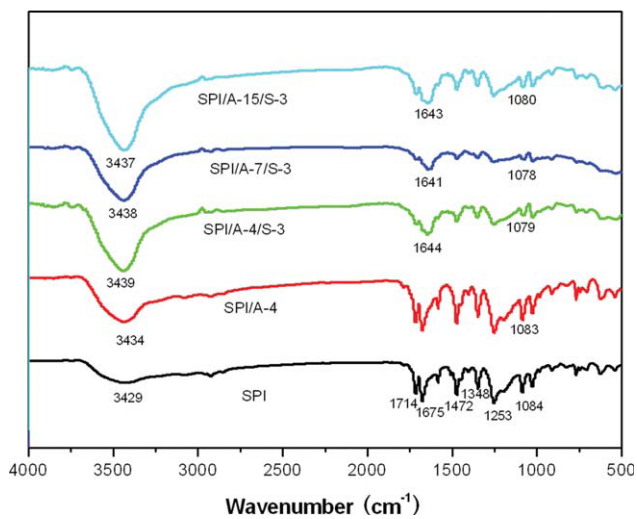

Figure 3 FTIR spectra of different hybrid membranes. [Color figure can be viewed in the online issue, which is available at wileyonlinelibrary.com.]

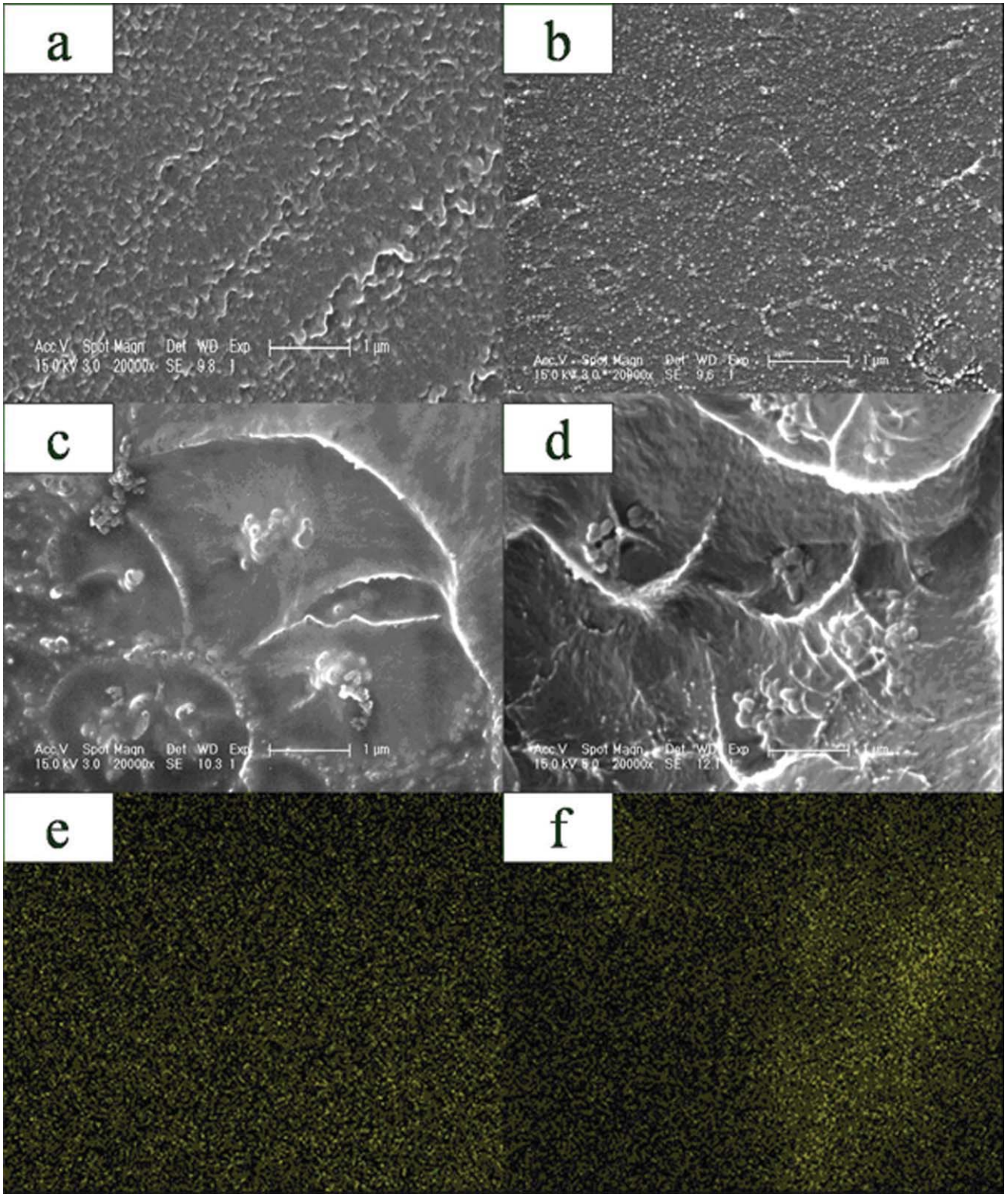

Figure 4 SEM images of SPI/A-4 (a), SPI/A-4/S-3 (b), SPI/A-15 (c), SPI/A-15/S-3 (d), Si-mapping distribution of SPI/A-4/S-3 (e) and SPI/A-15/S-3 (f).

shown in Figure S1. Figure 5 provides the typical TGA curves of three samples. It can be seen that the small weight loss below 200°C is attributed to the loss of moisture or residue solvents. The weight loss from 250°C to 400°C should be from the decomposition of sulfonic acid groups of SPI polymer, and the weight loss at higher temperature is caused by the degradation of SPI main chains. It deserves

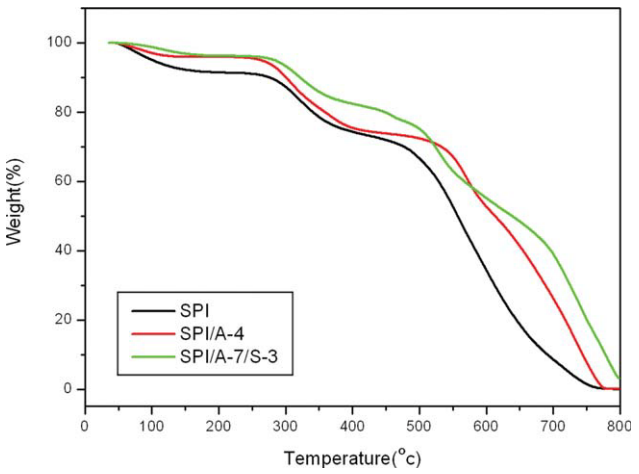

Figure 5 TGA curves of SPI and different hybrid membranes. [Color figure can be viewed in the online issue, which is available at wileyonlinelibrary.com.]

mentioning that although a roughly similar decomposition behavior is observed for these membranes, but the presence of SiO_2 networks derived from APTES and S-mSiO_2 results in a slightly increased thermal stability of SPI membrane at the second degradation stage. It is reasonable to assume that at 800°C, the —Si—O—Si groups in the hybrid membranes are converted to silica as no other components will survive at this high temperature. The experimental and theoretical values for the weight percent of residues for different samples are shown in Table I. The experimental values are higher than that of theoretical calculation prediction, indicating that the organic moieties do not completely decompose at 800°C. This is likely due to their entrapment by the inorganic phase, which gives rise to the apparent increased stability of the organic phase.

Tensile measurements

The mechanical properties of the nanocomposite membrane samples were measured using a tensile testing instrument at room temperature under 30% relative humidity and the results are listed in Table I. The Young's Modulus of the membranes is in the range from 876 to 1510 MPa. All the membranes show the elongations at break between 8.86 and 9.34%, and the tensile strengths from 43.1 to 47.4 MPa. Moreover, the mechanical properties for the prepared membranes seemed to be better than Nafion membrane. These datas indicate that the SPI/APTES/S-mSiO_2 membranes are strong and tough enough to be used in PEMs.

Ion exchange capacity

The IEC value which is an indication of the density of sulfonic acid groups in membranes was determined by titration. The IEC values of all the membranes are listed in Table II. The IEC values of hybrid membranes decrease with the increasing silica content. The reduction of IEC is mainly attributed to the dilution effect of the APTES phase and S-mSiO_2. This effect decreases the density of sulfonic acid groups in membranes. But all the SPI-based membranes exhibit the higher IEC values than that of Nafion 117, which is helpful for the improvement of the proton conduction and water uptake.

Water uptake

The water uptake is an important factor that directly affects the proton transportation in proton-conducting membranes. Generally, it is believed that the protons can be transported along with cationic mixtures such as H_3O^+ and $H_5O_2^+$ in the aqueous medium. The measured water uptakes of the SPI hybrid membranes are shown in Table II. It is worth noting that the SPI/APTES hybrid membranes have lower water-uptake than the pure SPI membrane, and the water uptake of the membranes decreases with the increasing amount of APTES. The formation of ionic crosslinking between –SO_3H of SPI and

TABLE I
Mechanical and Thermal Properties of Different Hybrid Proton Exchange Membranes

Sample[a]	Tensile strength (MPa)	Modulus (MPa)	Elongation (%)	Residue at 800°C (Experimental) (wt %)	Residue at 800°C (Theoretical) (wt %)
SPI	44.5	880	9.57	0.47	0
SPI/A-4	44.8	891	9.53	1.23	1.09
SPI/A-15	43.1	876	9.34	5.15	4.07
SPI/A-7/S-3	46.6	1170	9.49	3.78	3.17
SPI/A-15/S-3	47.4	1510	8.86	8.12	5.34
Nafion117	30.3[38,39]	357[38,39]	270[38,39]	–	–

[a] SPI, sulfonated polyimides; SPI/A-X/S-Y, where *X*, *Y* is the weight percent of APTES and S-mSiO_2, respectively.

TABLE II
Other Properties of Different Hybrid Proton Exchange Membranes

Sample	IEC (mmol/g)	Selectivity[a] (10^4S s/cm^3)	Water uptake (wt %)	Proton conductivity (S cm^{-1})			Methanol permeability (10^{-6} cm^2/s)
				25°C	40°C	80°C	
SPI	1.93	1.91	40.6	0.141	0.154	0.179	7.40
SPI/A-4	1.90	2.70	39.5	0.140	0.151	0.172	5.16
SPI/A-7	1.85	3.22	38.8	0.128	0.143	0.157	3.97
SPI/A-15	1.79	2.37	38.6	0.119	0.131	0.146	5.01
SPI/A-4/S-3	1.87	3.16	44.5	0.148	0.161	0.184	4.68
SPI/A-7/S-3	1.80	4.70	43.7	0.143	0.159	0.180	3.04
SPI/A-15/S-3	1.76	3.19	42.3	0.132	0.156	0.173	4.14
S-mSiO_2	1.42	–	–	–	–	–	–
Nafion 117[a]	0.91	1.09	35.0	0.096	0.138	0.176	8.80

[a] Data measured in our laboratories with the same condition as hybrid membranes.

–NH_2 of APTES would result in a more compact microstructure that could decrease the size of the hydrophilic ionic clusters.[28] Therefore, the water uptake decreases after APTES is added. But in the hybrid membranes of SPI/APTES/S-mSiO_2, the water uptake increases dramatically. It is known that besides the sulfonic acid groups in S-mSiO_2, the high surface area of mesophase structure of S-mSiO_2 can also increase the content of water. So, the increasing water uptake in SPI/APTES/S-mSiO_2 is mainly due to the strongly hygroscopic effect of S-mSiO_2.

Proton conductivity and methanol permeability

The proton conductivities of the hydrated membranes are listed in Table II and plotted as a function of temperature (Fig. S2). As seen, the proton conductivities of all the membranes increase in proportion to the measuring temperature. The proton conductivities of the hybrid membranes SPI/APTES are some lower than that of pure SPI membrane. This result should be attributed to the following two reasons. First, with the increase of APTES content, more sulfonic acid groups were used to establish ionic crosslinking with the amine groups of APTES; thereby losing their partial functionality for proton generation and conduction. Second, an increase in the APTES content would decrease the uptake of water and IEC, which is needed for proton transport. But in membranes of SPI/APTES/S-mSiO_2, the proton conductivities are higher than that of SPI/APTES. For example, the proton conductivity of SPI/A-4 is 0.172 S cm^{-1} at 80°C, while this value of SPI/A-4/S-3 is 0.184 S cm^{-1} at the same testing condition. The increase of the proton conductivity is possiblely due to the synergistic effect between the hydrated sulfonic group and the water molecules absorbed by the hydrated mesoporous silica particles. The proton from the activated H_2O:H^+ state dissociates to form a new activated state with a neighboring H_2O, which facilitates the proton transport ability through the mesoporous structure by the Grotthus mechanism, originated by the generation of a continuous proton conductive pathway.[40]

To prevent fuel from penetrating and energy efficiency loss, the proton exchange membranes used in direct methanol fuel cells should possess well methanol resistance property. All the hybrid membranes have the lower methanol permeability than Nafion117. For example, the membrane of SPI/A-7/S-3 shows the lowest methanol permeability of 3.04 $\times$ 10^{-6} cm^2 s^{-1}, while the value of Nafion117 is 8.80 $\times$ 10^{-6} cm^2 s^{-1}. The decrease in methanol permeability is the consequence of the establishment of acid–base ionic crosslinking and the presence of dispersed mesoporous silica particles. The former leads to the densification of the membrane structure and the latter increases the barrier to methanol passage. Meanwhile, the dispersed S-mSiO_2 inorganic fillers into polymeric matrices make the tortuous pathways (see Scheme 2), which results in high barrierity against methanol molecules.[41]

The selectivity, that is, the ratio of proton conductivity to methanol permeability, is a crucial factor for polymer electrolyte membranes to be used in direct methanol fuel cells. Accordingly, higher selectivity could allow superior membrane performance. As seen in Table II and Figure S3, all the hybrid membranes have the higher selectivity in the range 2.37 $\times$ 10^4 to 4.70 $\times$ 10^4 S s cm^{-3} at 25°C, while pure SPI has the value of 1.91 $\times$ 10^4 S s cm^{-3} at the same temperature. This result indicates that the cross-linking process can greatly improve the selectivity of membranes. The improvement of the selectivity could be resulted from that the cross-linking effectively hinders the polymer chain mobility and suppresses the swelling of membranes, which may be responsible for the reduced methanol permeability and the improved selectivity.

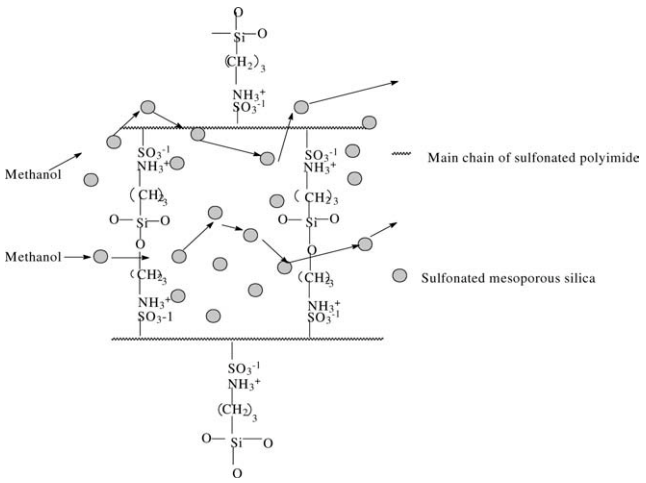

Scheme 2 Schematic illustration for the methanol permeability of hybrid membranes.

CONCLUSIONS

A series of hybrid proton-conducting membranes based on sulfinated polyimide (SPI) and aminopropyltriethoxysilane (APTES) doping with sulfonated mesoporous silica (S-mSiO_2) were prepared by the casting procedure. The crosslinking networks originated from APTES together with the doped sulfonated mesoporous silica improved the thermal stability of the hybrid membranes. The composite membranes doped with sulfonated mesoporous silica nanoparticles displayed superior comprehensive performance to the SPI and SPI-APTES membranes. The homogeneously dispersed S-mSiO_2 provided new pathways for proton transport, and rendered more tortuous pathways as well as greater resistance for methanol crossover. All the hybrid membranes showed the higher selectivity in the range from 2.37×10^4 to 4.70×10^4 S s cm^{-3} at 25°C, while Nafion117 was 1.09×10^4 S s cm^{-3}.

References

1. Devanathan, R. Energy Environ Sci 2008, 1, 101.
2. Hickner, M. A.; Ghassemi, H.; Kim, Y. S.; Einsla, B. R.; McGrath, J. E. Chem Rev 2004, 104, 4587.
3. Kim, Y. J.; Choi, W. C.; Woo, S. I.; Hong, W. H. J Membr Sci 2004, 238, 213.
4. Costamagna, P.; Srinivasan, S. J Power Sources 2001, 102, 242.
5. Chikh, L.; Delhorbe, V.; Fichet, O. J Membr Sci 2011, 368, 1.
6. Chai, Z. L.; Wang, C.; Zhang, H. J.; Doherty, C. M.; Ladewig, B. P.; Hill, A. J.; Wang, H. T. Adv Funct Mater 2010, 20, 4394.
7. Lin, B. C.; Cheng, S.; Qiu, L. H.; Yan, F.; Shang, S. M.; Lu, J. M. Chem Mater 2010, 22, 1807.
8. Mauritz, K. A.; Moore, R. B. Chem Rev 2004, 4, 4535.
9. Wu, D.; Xu, T. W.; Wu, L.; Wu, Y. H. J Power Sources 2009, 186, 286.
10. Guo, M. M.; Liu, B. J.; Guan, S. W.; Li, L.; Liu, C.; Zhang, Y. H.; Jiang, Z. H. J Power Sources 2010, 195, 4613.
11. Tripathi, B. P.; Shahi, V. K. Prog Polym Sci 2011, 36, 945.
12. Carretta, N.; Tricoli, V.; Picchioni, F. J Membr Sci 2000, 166, 189.
13. Park, H. B.; Lee, C. H.; Sohn, J. Y.; Lee, Y. M.; Freeman, B. D.; Kim, H. J. J Membr Sci 2006, 285, 432.
14. Xiao, L. X.; Zhang, H. F.; Scanlon, E.; Ramanathan, L. S.; Choe, E. W.; Rogers, D.; Apple, T.; Benicewicz, B. C. Chem Mater 2005, 17, 5328.
15. Schuster, M.; Araujo, C. C. D.; Atanasov, V.; Andersen, H. T.; Kreuer, K. D.; Maier, J. Macromolecules 2009, 42, 3129.
16. Wu, D.; Fu, R. Q.; Xu, T. W.; Wu, L.; Yang, W. H. J Membr Sci 2008, 310, 522.
17. Sen, U.; Celik, S. U.; Ata, A.; Bozkurt, A. Int J Hydrogen Energy 2008, 33, 2808.
18. Reichman, S.; Burstein, L.; Peled, E. J Power Sources 2008, 179, 520.
19. Acar, O.; Sen, U.; Bozkurt, A.; Ata, A. Int J Hydrogen Energy 2009, 34, 2724.
20. Smitha, B.; Devi, D. A.; Sridhar, S. Int J Hydrogen Energy 2008, 33, 4138.
21. Yoshimura, K.; Iwasaki, K. Macromolecules 2009, 42, 9302.
22. Tsang, E. M. W.; Zhang, Z. B.; Shi, Z. Q.; Soboleva, T.; Holdcroft, S. J Am Chem Soc 2007, 129, 15106.
23. Zhang, F.; Li, N. W.; Zhang, S. B.; Li, S. H. J Power Sources 2010, 195, 2159.
24. Terraza, C. A.; Liu, J. G.; Nakamura, Y.; Shibasaki, Y. J.; Ando, S.; Ueda, M. J Polym Sci Part A: Pol Chem 2008, 46, 1510.
25. Zhang, Y.; Wan, Y.; Zhao, C. J.; Shao, K.; Zhang, G.; Li, H. T.; Lin, H. D.; Na, H. Polymer 2009, 50, 4471.
26. Nagarale, R. K.; Shin, W.; Singh, P. K. Polym Chem 2010, 1, 388.
27. Oh, Y. S.; Lee, H. J.; Yoo, M.; Kim, H. J.; Han, J.; Kim, T. H. J Membr Sci 2008, 323, 309.
28. Xue, Y. H.; Fu, R. Q.; Wu, C. M.; Lee, J. Y.; Xu, T. W. J Membr Sci 2010, 350, 148.
29. Kundu, P. P.; Kim, B. T.; Ahn, J. E.; Han, H. S.; Shul, Y. G. J Power Sources 2007, 171, 86.
30. Hsiao, J. K.; Tsai, C. P.; Chung, T. H.; Hung, Y.; Yao, M.; Liu, H. M.; Mou, C. Y.; Yang, C. S.; Chen, Y. C.; Huang, D. M. Small 2008, 4, 1445.
31. Stromme, M.; Brohede, U.; Atluri, R.; Garcia-Bennett, A. E. Nanomed Nanotechnol 2009, 1, 140.
32. Nooney, R. I.; Dhanasekaran, T.; Chen, Y. M.; Josephs, R.; Ostafin, A. E. Adv Mater 2002, 14, 529.
33. Pattantyus-Abraham, A. G.; Wolf, M. O. Chem Mater 2004, 16, 2180.
34. Tominaga, Y.; Hong, I. C.; Asai, S.; Sumita, M. J Power Sources 2007, 171, 530.
35. Choi, Y.; Kim, Y. K.; Kim, H. K.; Lee, J. S. J Membr Sci 2010, 357, 199.
36. Okamoto, K. I.; Yaguchi, K.; Yamamoto, H.; Chen, K. C.; Endo, N.; Higa, M.; Kita, H. J Power Sources 2010, 195, 5856.
37. Fang, J. H.; Guo, X. X.; Harada, S.; Watari, T.; Tanaka, K.; Kita, H.; Okamoto, K. Macromolecules 2002, 35, 9022.
38. Liu, H. D.; Zhao, C. J.; Jiang, Y. N.; Ma, W. J.; Na, H. J Power Sources 2010, 195, 762.
39. Rhima, J. W.; Park, H. B.; Lee, C. S.; Jun, J. H.; Kim, D. S.; Lee, Y. M. J Membr Sci 2004, 238, 143.
40. Siu, A.; Schmeisser, J.; Holdcroft, S. J Phys Chem B 2006, 110, 6072.
41. Hasani-Sadrabadi, M. M.; Dashtimoghadam, E.; Majedi, F. S.; Kabiri, K.; Solati-Hashjin, M.; Moaddel, H. J Membr Sci 2010, 365, 286.